American Journal of Nano Research and Applications
2016; 4(3): 23-32
http://www.sciencepublishinggroup.com/j/nano
doi: 10.11648/j.nano.20160403.11

Studies on the Influence of Growth Time on the Rutile TiO_2 Nanostructures Prepared on Si Substrates with Fabricated High-Sensitivity and Fast-Response p-n Heterojunction Photodiode

Abbas M. Selman[1, 2]

[1]Department of Pharmacognosy and Medicinal Plants, Faculty of Pharmacy, University of Kufa, Najaf, Iraq

[2]Institute of Nano Optoelectronic Research and Technology (INOR), University Sains Malaysia, Penang, Malaysia

Email address:
alabbasiabbas@yahoo.co.uk

To cite this article:
Abbas M. Selman. Studies on the Influence of Growth Time on the Rutile TiO_2 Nanostructures Prepared on Si Substrates with Fabricated High-Sensitivity and Fast-Response p-n Heterojunction Photodiode. *American Journal of Nano Research and Applications*. Vol. 4, No. 3, 2016, pp. 23-32. doi: 10.11648/j.nano.20160403.11

Received: October 23, 2016; **Accepted**: November 8, 2016; **Published**: January 10, 2017

Abstract: In this study, the effect of duration on the growth of rutile TiO_2 nanostructures (Ns) deposited onto the p-Si (111) substrate on the structural, morphological, and optical properties of rutile TiO_2 Ns has been investigated. All Si substrates were seeded with a TiO_2 seed layer synthesized using a radio-frequency (RF) reactive magnetron sputtering system. Chemical bath deposition method (CBD) was employed to grow rutile TiO_2 Ns on seeded Si substrates at duration time of growth (1, 2, 3, and 4 h). X-ray diffraction, Raman spectroscopy, and field-emission scanning electron microscopy (FESEM) analyses demonstrated the tetragonal rutile structure of the synthesized TiO_2 Ns with the highest (110) peak intensity. Optical properties were investigated by using photoluminescence (PL) spectroscopy of the grown rutile Ns, with the spectra exhibiting the sharpest (smallest FWHMs) and highest peak revealed the high quality of TiO_2 Ns with few defects was found for the sample prepared for 3 h, which reflects the crystalline quality. These results show that the optimized growth conditions yield very high quality TiO_2 Ns on p-type (111)-oriented silicon substrates. A fast-response p-n heterojunction photodiode was fabricated by depositing Al contacts on the front of the optimal sample via RF reactive magnetron sputtering. Upon illumination of a pulsed UV light (325 nm, 1.6 mW/cm^2) at 5 V bias voltage, the device showed 3.8×10^2 sensitivity, the photoresponse peak was 460 mA/W, the response and recovery times were 50.8 and 57.8 ms, respectively.

Keywords: Titanium Dioxide, Rutile Nanostructures, Chemical Bath Deposition, Growth time, Photodiode

1. Introduction

Titanium dioxide (TiO_2) is an important semiconductor material with a wide band gap (3.02 eV for rutile and 3.20 eV for anatase) and it is an n-type semiconductor [1]. TiO_2 exists in three crystal structures, namely, anatase, rutile, and brookite. The rutile phase exhibits high hardness, Young's modulus, refractive index, dielectric constant, transparency in the visible region, ultraviolet (UV) absorption rate, and chemical stability, as well as excellent mechanical strength [2, 3]. These properties increase the demand for the rutile form of TiO_2 as a research material for various applications, including sensing [4], photocatalysis [5, 6], solar cells [7], light-emitting diodes [8], and UV detectors (UV-PD_c) [9]. Currently, one-dimensional TiO_2 nanostructures (Ns) can be grown by thermal evaporation [10], hydrothermal synthesis [11], template synthesis [12], sol–gel method [13], chemical vapor deposition [14], electrochemical deposition [15], and chemical bath deposition (CBD) [16]. Among these methods, CBD is a promising and flexible approach because of its simple and low-cost process for synthesizing TiO_2 Ns with controllable morphology [17]. The effect of duration time on the size and structure of crystalline TiO_2 has been investigated by many researchers [18]. Zhao et al. [19] studied the influence of growth time and annealing on rutile TiO_2 single-crystal nanorod arrays on FTO substrate via

hydrothermal method. They concluded that increasing the growth time hardly induced an obvious change in NR length because the precursor was progressively depleted with increasing reaction time. Regonini and Clemens. [20] investigated the influence of anodizing time on the length, morphology, and photoelectrochemical properties of TiO_2 nanotubes (NTs). They found that the optimum anodizing time was 20 min at 30 V and produced 1.1 μm long NTs films. A photocurrent density of 460 mA. cm^{-2} was generated. Altomare et al. [21] reported the effect of the anodization time on the structural features and photoactivity of TiO_2 NTs arrays prepared via electrochemical anodization. They concluded that the anodization time length has a key function in the preparation of well-aligned NTs arrays to be employed as photoactive materials in a variety of applications. Bandgar et al [22]. developed a simple, fast, and cost-effective method for the controllable synthesis of nanocrystalline TiO_2 at mild chemical reaction conditions without using an expensive experimental technique, which presented significant advantages. They studied the effect of reflux time on the fabrication of nanocrystalline TiO_2 prepared via a wet chemical synthesis route by using peroxotitanate complex solutions. They observed that increasing the reflux time resulted in variations in the crystalline size of TiO_2 in a systematic manner, and the reflux time has a substantial influence on the formation of nano TiO_2 with changing refractive indices and band gap energies. Cheng et al. [23] investigated the influences of various hydrothermal conditions such as pH, concentration of $TiCl_4$ solution, growth time, and temperature on the formation, phase, morphology, and grain size. They observed that the high acidity and concentration of $TiCl_4$ solution were beneficial in the formation of the rutile phase. The temperature had a strong effect on the grain size of the products and the agglomeration among grains. Lowering the temperature resulted in a decrease in grain size and an increase in agglomeration among grains. Furthermore, increasing the reaction time improved grain growth. The results showed that the average grain size of the products increased with increasing reaction time. The photoelectric, optical, and morphological properties of TiO_2 Ns have generated considerable attention from researchers because of their large specific surface area, distinctive UV absorption, and well-defined charge carriers transport path. Therefore, TiO_2 Ns are extremely appropriate for UV-PD_c against the background of infrared and/or visible light [24]. Aksoy et al. [25] formed an n-TiO_2 Ns/p-Si heterojunction diode based on TiO_2 Ns deposited on p-Si substrates via the sol–gel method by using the spin coating technique at deposition temperatures from 700°C to 1100°C. They noted that the crystallization of the anatase phase, which eventually transformed to rutile phase, occurred at 800°C. Furthermore, the Schottky barrier height (S_{BH}) and ideality factor (n) of n-TiO_2 Ns/p-Si heterojunction diode were 0.58 eV and 5.39, respectively. Therefore, these results exhibited that this device can be considered as a candidate for semiconductor device applications. Chang et al. [26] studied the heterojunction effects on the UV photoresponse of TiO_2 NTs fabricated using anodic aluminum oxide as a template and via atomic layer deposition nanotechnology on a Si substrate with ITO as the electrode. The study revealed that the photocurrent (I_{Ph}) produced by the ITO-TiO_2heterojunction (Schottky contact) was equal to the I_{Ph} produced by the TiO_2-Si heterojunction (p-n junction) at bias voltages from 0 V to -1 V. These results indicated the presence of a depletion region in the ITO-TiO_2 and Si-TiO_2heterojunctions. In other words, the diode transitioned from TiO_2-Si heterojunction-controlled to ITO-TiO_2heterojunction-controlled when the applied biases were changed from approximately 0 V to -1 V on the ITO electrode because the I_{Ph} produced from the ITO - TiO_2 heterojunction was improved at an increased reverse bias, whereas the current produced from the TiO_2-Si heterojunction decreased at an increased forward bias. The two I_{Ph} reached equal values at the transition point, thereby cancelling each other out. Zhang et al. [27] synthesized TiO_2 NWs arrays on FTO via hydrothermal method, which was modified with the deposition of ZnO via the crystallization method. They fabricated UV-PD_c based on TiO_2/ZnO heterojunction, which possessed high photoelectric performance. The ratio of I_{Ph} to dark current (I_d) was four orders of magnitude higher and the device had a high responsivity.In this work, to investigate the effect of duration on the growth of rutile TiO_2 Ns deposited onto the seeded p-Si (111) substrate, four duration times have been studied (1, 2, 3, and 4 h). The optimum deposition time was also determined. The optimal structural properties were selected to fabricate UV photodiode (UV-PD_i), and its photoelectric characteristics were studied.

2. Experimental Details

2.1. TiO_2 Seed Layer Preparation on Different Substrates

The seed layers of TiO_2 were prepared with radio frequency (RF) reactive magnetron sputtering on p-type silicon (Si) (111) substrates for 80 min, with a thickness of approximately 100 nm ± 5 nm. The target of TiO_2 is a disk with high purity (99.99%, 3 in diameter). To clean the TiO_2 disk surface, the target was presputtered for 5 min before deposition. Prior to deposition, the Si substrates were cleaned with a wet chemical etching with Radio Corporation of America (RCA) method described in our previous work [28]. After the chamber was evacuated below 2×10^{-5} mbar with an RF power of 150 W, the high-purity argon (99.99%) was used as sputtering gas at a fixed ratio of 17%. The seed layer deposition was then performed under a total pressure of 3×10^{-3} mbar. The substrates were deposited onto a heated substrate at 350°C at an average deposition rate of 0.2 Å/s. Then, these seeded substrates were annealed at 550°C for 1 h in air to improve crystallinity.

2.2. TiO_2 Nanostructure Growth

The seed layer of TiO_2-coated Sisubstrates was cleaned in an ultrasonic bath with acetone solution, rinsed with distilled water, and dried with nitrogen gas. CBD was used to

synthesize TiO_2Ns by heating an acidic solution of $TiCl_3$, which contained an immersed seed layer of TiO_2-coated substrates. The growth conditions of TiO_2 Ns followed our previous procedure [28-32]. In brief, approximately 4 ml of $TiCl_3$ liquid (15 wt% in HCl; Merck SdnBhd, Malaysia) was mixed with 50 ml distilled water. Urea (NH_2CONH_2; 0.1 M) was added to adjust pH media to approximately 0.7. After stirring for 1 h at room temperature (27°C), a homogeneous violet solution was obtained. The seeded Si substrates were then vertically inserted in the bath, which were then heated at 55°C. During the precipitation that initiated in the bath, a heterogeneous reaction occurred, and TiO_2 was deposited onto the substrates. When the growth time reached a set value, the substrates coated with TiO_2 Ns were removed from the solution bath, rinsed with distilled water, and then dried with nitrogen gas.Then, these prepared samples were annealed at 550°C for 2 h in air to improve crystallinity and to decompose $Ti(OH)_4$ into TiO_2 [33]. Furthermore, anatase, rutile, or mixtures of both phases might appear in the prepared samples. Therefore, an optimum annealing temperature (>500°C) is required additionally to convert anatase phase into rutile phase [34]. The surface morphology and structure of the prepared TiO_2Ns were characterized and analyzed with FESEM (Leo Supra 50VP, Carl Zeiss, Germany) equipped with an energy-dispersive X-ray (EDX) system and XRD (PANalyticalX'Pert PRO MRD PW3040) with CuK_α radiation (λ = 1.541 Å). The optical properties were measured at room temperature with a photoluminescence (PL) spectroscopy system (JobinYvon HR 800 UV, Edison, NJ, USA) with an He–Cd laser (325 nm, 20 mW) and a Raman spectrometer (Horiba JobinYuon HR 800UV, Edi-son, NJ, USA) with Ar^+ as the excitation source operated at a wavelength of 514.55 nm (20 mW). The monochromator was connected to the computer supplied with V4.01 of Cornerstone Utility Programming to select the desirable wavelength (UV light) from a 200W Hg (Xe) ozone-free lamp as a light source. Newport power meter (Model 2936-C USA) was used to calibrate the output power. A bias voltage was applied to the sample using DC power supply (GW InsTEK, model GPS 3030). The photocurrent was calculated by Autorangeing Microvolt DMM (Keithley, model 197A) at different wavelengths.

3. Results and discussion

3.1. Morphological and Structural Characterization of TiO_2 Ns

3.1.1. Surface Morphology

Fig. 1 shows the FESEM images of the TiO_2 Ns synthesized on p-type (111)-oriented silicon substrates with a TiO_2 buffer layer using CBD at different durations of growth. From Fig. 1 (a), for the sample prepared for 1 h, small and few well-defined flowers were found, with each flower consisting of bundles of short nanorods (NRs) with sharp tips and connected to each other such that estimating the diameter and average length of the NRs was difficult. The structure appeared slightly agglomerated, and voids were observed in almost the entire surface of sample. When the reaction was prolonged up to 2 h [Fig. 1(b)], structures, similar to those previously obtained, showed the increasing size of nanoflowers to be approximately 250 nm, which is more than twice the size of previous structures. Moreover, the voids decreased in this sample. As the growth time was prolonged to 3 h, uniform and high-density growth mix of NRs and nanoflowers emerged, with each petal of the nanoflowers assembled by several conical rods [Fig. 1(c)]. These NRs were 20–30 nm in diameter and 80–110 nm in length. At 4 h of growth time, the TiO_2 structure showed flower-like structures with random growth surface and some cracks, and the bundles of small NRs grew vertically and horizontally to the substrate [Fig. 1 (d)]. Compared with the images in Fig. 1, the TiO_2 density in Fig. 1(c) was much higher, and this structure provided the film with a large surface area, which indicated that the sample prepared for 3 h had more nucleation sites. Thus, different superstructures of rutile TiO_2 NRs can be obtained by controlling the duration of growth. Furthermore, the EDX spectra of all samples indicated the presence of Ti and O atoms in the thin layers, thereby confirming the formation of TiO_2 Ns. Figure 2 also demonstrates that the ratio of Ti-to-O was dependent on the duration of growth. The Ti-to-O ratios of the samples prepared at different growth durations are listed in Table 1. These ratios showed good stoichiometry compared with the other three samples grown for 3 h. Furthermore, the EDX revealed that this sample contained 50.06 wt% Ti and 49.94 wt% O, whereas the signal of Si came from the Si substrate.

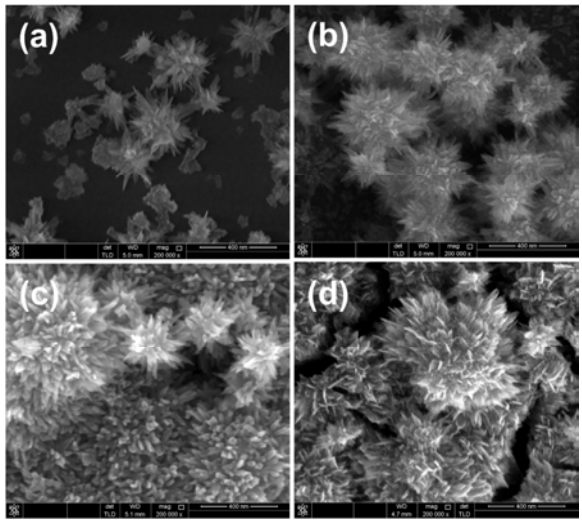

Fig. 1. *FESEM images of rutile TiO_2 Ns grown on p-type (111)-oriented silicon substrates at.*

Table 1. *The EDX spectra results of TiO_2 Ns grown on silicon (111) substrate atdifferent duration time of growth.*

Growth time (h)	Ti		O_2	
	weight %	Atom %	weight %	Atom %
1	30.88	12.98	69.12	87.02
2	51.26	26	48.74	74
3	50.06	25.08	49.94	74.92
4	49.5	23.93	51.5	76.07

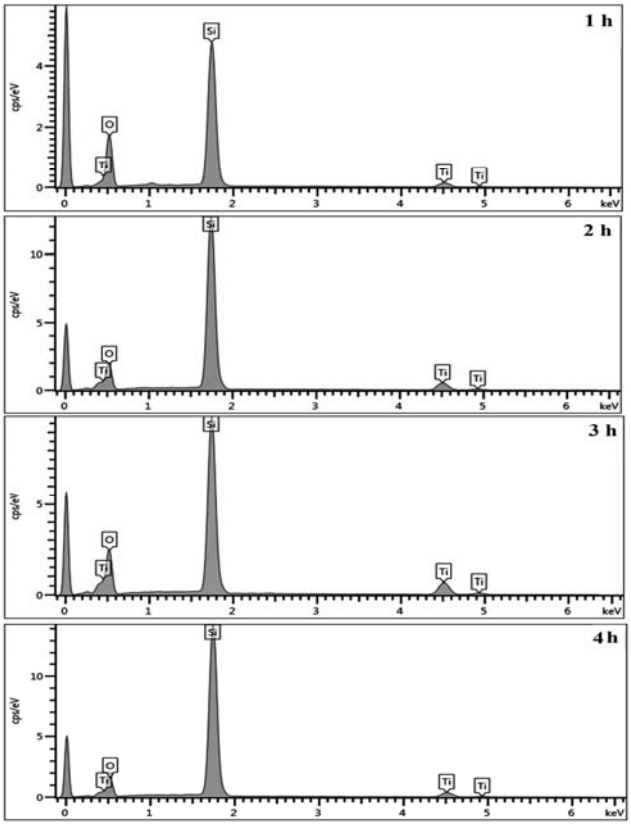

Fig. 2. *EDX spectra of TiO_2 Ns grown on silicon (111) substrate at different duration time of growth.*

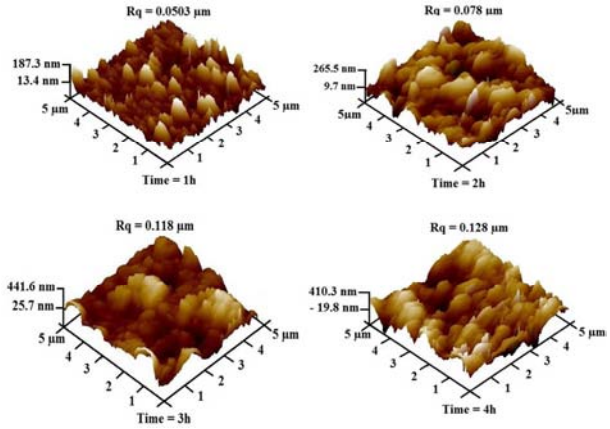

Fig. 3. *AFM images (3D) of the rutile TiO_2 Ns grown on silicon (111) substrate at different duration time of growth.*

Figure 3 shows the 3D AFM images (5 µm×5 µm) of the surface morphology of prepared TiO_2 Ns at different durations of growth (1, 2, 3, and 4 h). The high roughness of the film surfaces was evident. The R_{rms} values for the samples grown for 1, 2, 3, and 4 h were 0.0503, 0.078, 0.018, and 0.128 nm, respectively. The surface roughness increased with increasing deposition time. Hence, the denser films with uniform distribution of grains with high surface roughness were observed in the samples grown for 3 h. This increase in roughness is due to an increase in the grain size [35]. The grain size has been evaluated using Scherrer formula [36]. The estimated grain sizes are about 8.55, 10.42, 10.5, and 8.33 nm for samples grown for 1, 2, 3, and 4 h respectively.The sample grown at 4 h exhibited a higher surface roughness (0.128 µm) compared with the others because of the possible etching from the HCl solution in the bath after prolonged growth. Thus, the chemical etching action from the HCl solution may be a direct and dominant reason for the detachment of rutile Ns [19]. Therefore, the duration of growth is suitable for controlling the surface morphology as well as for increasing the surface roughness and density of the material distribution on the surface.

3.1.2. Crystalline Structure

Films crystallinity were analyzed using X-ray diffraction. The XRD patterns of the TiO_2 Ns synthesized on seeded Si substrates at different durations of growth are shown in Fig. 4. All prepared samples fully fit well with the rutile TiO_2 phase (JCPDS card No.01-078-1508). Moreover, all samples exhibited sharper and stronger diffraction intensity peaks related to the (110) plane compared with those of (101), (211), and (301), indicating that their x-axis and y-axis orientations are parallel to the substrates. These distinct peaks were noted in the XRD patterns at 27.47°, 27.51°, 27.46°, and 27.47° for the rutile TiO_2 NRs grown for 1, 2, 3, and 4 h, respectively. All these peaks matched very well with the standard position (27.44°) of bulk rutile TiO_2 of the (110) plane ascribed to rutile. These results are in agreement with the previous study for rutile structure [37-40]. Compared with the other three samples, the diffraction peaks became sharper and narrower for the sample prepared for 3h, thereby indicating the enhancement of crystallinity and growth of nanocrystals [41].

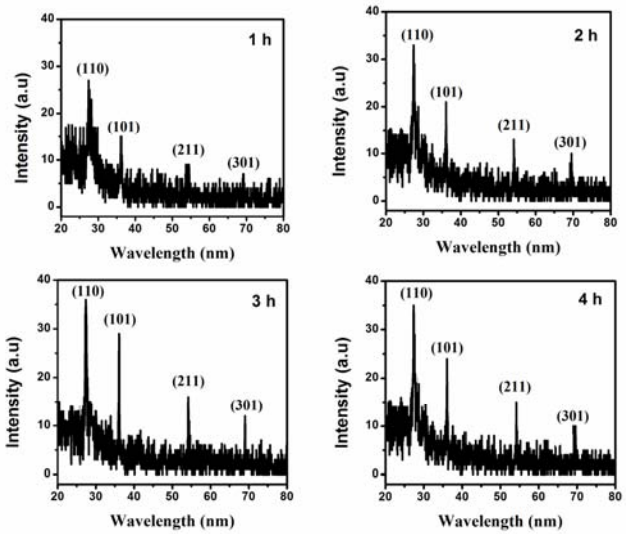

Fig. 4. *XRD patterns of TiO_2 Ns grown at different duration time of growth.*

3.2. Optical Properties

3.2.1. PL Spectra

Figure 5 shows the PL spectra of rutile TiO_2 Ns grown at different durations. For all prepared samples, the PL excitation spectra had a band around 421, 428, 417, and 405 nm corresponding to 2.95, 2.9, 2.97 and 3.06 eV for

the sample grown at 1, 2, 3, and 4 h, respectively, which agrees well with the value of the band gap energy of TiO_2 (~3.0 eV) for rutile [42, 43]. Therefore, this band indicates the photoabsorption near the edge of the conduction band. Although, the exact band positions of the PL excitation spectra slightly differed from each another, no significant change in the band gap was observed with increasing growth time. Clearly, the sharpest (smallest FWHMs) and highest peak was found for the sample prepared for 3 h, which reflects the crystalline quality; a smaller FWHM indicates a better crystal quality [44]. Therefore, this sample is the best one, which is consistent with the XRD results. The peaks at 527 nm (2.35 eV) were found for the samples prepared for 1 and 2 h, and the peaks at 527 (2.35 eV) and 703 nm (1.76 eV) for the sample prepared at 4h. These emissions were the radiative recombination of the self-trapped excitons and the radiative transitions inside the sub-states initiated from the TiO_2 surface [45]. This result agreed well with several studies that correlated the origin of these emissions band to the same reason stated above [46, 47]. The broad peaks that centered at approximately 820 (1.5 eV), 855 (1.45 eV), and 850 (1.46 eV) nm for the rutile grown for 1, 2 and 3 h, respectively, may be related to the intrinsic defects and interstitial oxygen, which occurred because of excessive oxygen in the synthesized rutile [48]. From these observations, the rutile TiO_2 Ns grown for 3 h possessed optimal optical properties.

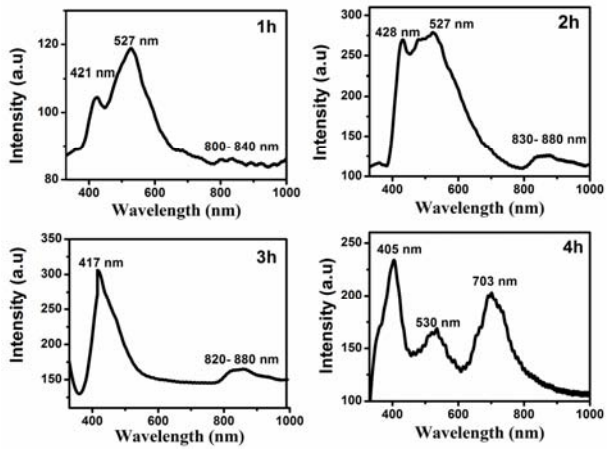

Fig. 5. Photoluminescence spectra at room temperature of the rutile TiO_2 Ns grown at different duration time of growth.

3.2.2. Raman Spectrum

Figure 6 shows the Raman spectra of the prepared TiO_2 Ns at different durations (1, 2, 3, and 4 h). The observed band positions and vibrational modes correspond to the rutile phase for all samples and agree with the reported values of the typical Raman bands of the rutile phase [49, 50]. The Raman spectra demonstrated the formation of rutile phase for all Ns films formed on the seeded Si substrates because the higher acidity of the solution facilitated the formation of rutile phase [50] and the annealing treatment for the seed and samples prepared (550°C) was also required to convert anatase phase into rutile phase [34]. No significant change in the position of these peaks was observed. During the first hour of growth, very few nanoflowers were formed on the substrate [Fig. 1(a)]. Moreover, increased amount and size of the nanoflowers were found on the substrate grown for 2 h [Fig. 1(b)]. Therefore, the intensities of the Raman bands at 230, 441, and 614 cm^{-1}, as well as those at 239, 441, and 614 cm^{-1}, appeared very weak. When the reaction was prolonged to 3 h, the intensities of the Raman bands at 237, 447, and 612 cm^{-1} dramatically increased. This result indicated that the thickness and density of the TiO_2nanoflowers films increased because of the increase in the duration of growth [50] as shown in Fig. 1 (c). By contrast, when the duration time was increased to 4 h, the density of the rutile nanoflowers grown on the substrate decreased, and the large cracks separated the film into several unattached areas [Fig. 1(d)], because the precursor in the solution was depleted gradually with increased reaction time [51]. Therefore, the intensities of the Raman bands at 236, 447, and 612 cm^{-1} slightly decreased. In addition, the strong band at 520 cm^{-1} and a weak broad band placed between 945 cm^{-1} and 985 cm^{-1} originated from the Si substrate, which is in agreement with previous findings for Si substrate [36]. These findings are also in agreement with the XRD results. Based on these XRD, FESEM, and Raman results, we assumed that the rutile TiO_2 Ns formed on the seeded Si substrates grown for 3 h promoted the nucleation and epitaxial growth of rutile Ns, and this condition is the optimal for the growth of high-quality rutile Ns.

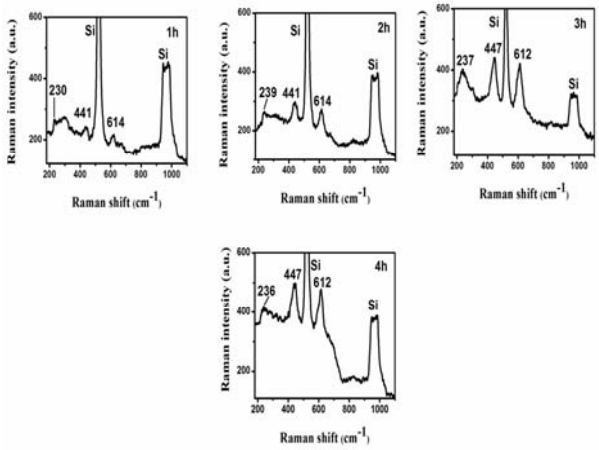

Fig. 6. Raman spectra of rutile TiO_2 Ns grown on silicon (111) substrate at duration time of growth.

3.3. Device Fabrication

The growth of rutile TiO_2 films on Si substrates with different deposition method attracted significant amount of attention because Si substrate is widely used in semiconductor industry [67, 68]. In addition to the preceding observations for optical and structural analyses, we conclude that the optimal sample of rutile NRs was the sample grown at 3h. The fabrication of the UV-PD_i device based on the optimal samplewas conducted by depositing Al finger

contact (approximately 100 nm thickness) on top of TiO_2 NRs by using a metal mask. The schematic of the device structure is shown in Fig. 7. Indium metallization (approximately 200 nm thickness) was deposited onto the back side of the p-Si. Both electrodes (back and front contacts) were deposited using RF reactive magnetron sputtering, where the chamber was evacuated below 3×10^{-5} mbar with an RF power of 50 and 120 W for In and Al, respectively. High-purity Ar was used as a sputtering gas at a fixed ratio of 17%. Deposition was then performed under a total pressure of 3×10^{-3} mbar. The contacts were deposited at room temperature, then; the thermal annealing processes were conducted for the metallic contact at 300°C for 20 min with N_2 gas to produce homogenous ohmic contacts. N_2 gas was used inside the tube furnace during annealing of metal contacts to avoid oxidation, where the ambient room and tube furnace contains O_2 molecules. The active area of the Pt/TiO_2NRs/P-Si (111)/In heterojunction photodiode (PD_i) was about 0.39 cm^2.

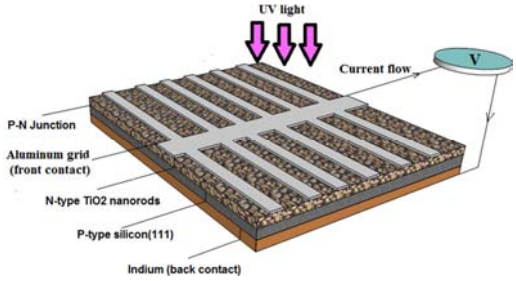

Fig. 7. *Current-voltage characteristics of the TiO_2NRs/p-Si (111) heterojunction UVphotodiode under dark and UV illumination (325 nm, 1. 6 mW/cm^2).*

3.4. Current–Voltage Characteristics

Dark and photocurrent measurements are performed for the fabricated Al/TiO_2NRs/p-Si (111)/In heterojunction PDi, which is illustrated in Fig. 8, were studied by measuring the current–voltage (I–V) relationships with rectifying ratio (If/Ir) of 254 and 95 at –5 V and 5 V bias voltages. The study was performed in the dark and under UV light illumination (325 nm, the incident optical power was 1.6 m W/cm2 at a distance of 3 cm from the UV lamp). Under UV illumination, an applied bias voltage of 5 V at the rutile TiO_2 NRs-Si junction produced an electric field in the depletion region. This region contained a high number of electrons that moved toward TiO_2 and a high number of holes that migrated toward the Si substrate; high photocurrent then formed and rapidly moved into the external circuit through the electrodes, as shown in Fig. 8 [52]. The device placed in the dark produced current, which was six times smaller than the current obtained under UV illumination. This finding indicated that the PD of TiO_2NRs/P-Si (111) exhibited excellent light response. The current was kept nearly constant at a small bias (Vbias< 0.5 V). These results indicated that the charge carriers produced during UV illumination at high bias voltage (Vbias> 0.5 V) determined the current produced and caused increased current. However, the current was not sensitive to UV illumination when a small bias was applied because the current of the device was restricted by the depletion region between n-TiO_2 and p-Si. Therefore, the TiO_2 NRs absorbed UV light and generated electron–hole pairs in the depletion region. The presence of an electric field in the depletion region caused by an applied bias voltage (Vbias> 0.5 V) resulted in the separation of charge carriers, where the holes moved to the p-side and the electrons moved to the n-side. Thus, a photocurrent was generated at the external contact [53].

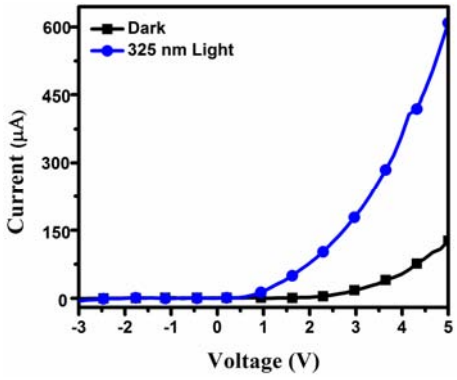

Fig. 8. *The schematic diagram of the device.*

The large difference between I_{ph} and I_d was attributed to the short transit time of charge carriers with long lifetime. The presence of O caused hole trap states at the TiO_2 NRs surface, which prevented the generation charge carrier pair (e^- –h^+) recombination and extended the lifetime of holes [54]. The PD_i sensitivity (S) was calculated using Eq. (1) [55]:

$$S(\%) = \frac{(I_{Ph} - I_d)}{I_d} \times 100 \quad (1)$$

The S value was 3.8×10^2 at 325 nm, and the light intensity was 1.6 m W/cm^2. Meanwhile, the applied bias voltage was 5 V. In general, responsivity (R) is a critical parameter that determines the sensitivity of a P D_i device. R is defined as the device photocurrent (I_{Ph}) generated per unit power of incident light (P_{inc}) on the effective area of the device (A) and can be expressed using Eq. (2) [54, 56-60]:

$$R = \frac{I_{Ph}(A)}{P_{inc}(W)} = \frac{I_{Ph}(A)}{E(W/Cm^2)A(Cm^2)} \quad (2)$$

Where E is the irradiance of UV light, which is measured by a standard UV power meter (Newport Power meter, Model 2936-C USA). The responsivity spectra of the fabricated P D_i were measured under front illumination within the range of 300 nm to 500 nm at 5 V-bias voltage (as shown in Fig. 9). Figure 9 demonstrates that photocurrent increased at wavelengths up to 310 nm, and then sharply decreased at wavelengths up to 350 nm. When the wavelength decreases, absorption coefficient increases the penetration depth and the UV light will be short. This process increases the concentration of the charge carrier pair near the TiO_2 NRs surface. Consequently, the lifetime of photogenerated carriers declined and responsivity decreased.

Under irradiation of 325 nm UV light, the peak photoresponse was 460 mA/W, which was more than 30 times higher than those reported for TiO_2-based Schottky-type UV light detector at around 330 nm [60]. This high R value was attributed to the TiO_2 NRs that provided high density with large and rough surface areas and the good p–n junction that formed in the TiO_2NRs/p-Si (111) [61]. Repeatability of the P $D_i$was studied by investigating the optical response using dynamic response time measurement by illuminating the P D_i to a pulsed UV light (325 nm, 1.6 m W/cm^2) at 5 V-bias voltage. Figure 10 shows the corresponding increase in photocurrent as a function of time when the UV light was repeatedly switched on and off 17 times (partially shown in Fig. 10). The results showed acceptable difference with time. The curves in Fig. 10 reveal rectangular-shaped profiles, and the magnitudes of photocurrent in every on/off cycle are steady and repeatable. The response time (i.e., the time in which current increased from 10% to 90% of its saturation value) and recovery time (i.e., the time in which current decreased from 90% and back to 10% of its saturation value) for P D_i were measured at various bias voltages, as shown in Fig. 10. The response time and recovery time of the NRs in this study were clearly by far the shortest time achieved in various TiO_2 UV detectors reported in the literature [62-64]. The extremely fast PD_i photoresponse in the current study was related to the high quality and large photoactive surface areas of the TiO_2 NRs grown on p-type Si substrate. The fast response indicated that the vertical TiO_2 NR PD_i was useful in high-speed operation. Moreover, the high value of photocurrent and responsivity were ascribed to several carriers that were collected under illumination in the TiO_2 NRs films. This finding was in agreement with results of a previous study, which showed exceptional photoactivity of nanostructures. This result explained the sensitivity and stable performance of the NRs during UV light detection [65]. The findings revealed that Al/TiO_2NRs/p-Si (111)/In heterojunction PD exhibited potential application as a UV detector.

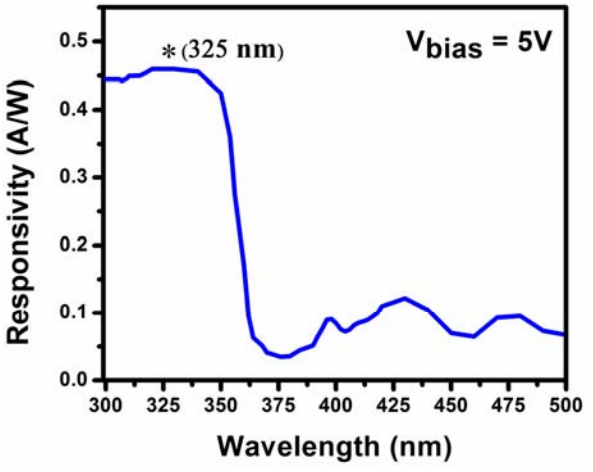

Fig. 9. Theresponsivity spectra of the TiO_2NRs/p-Si (111) heterojunction photodiode.

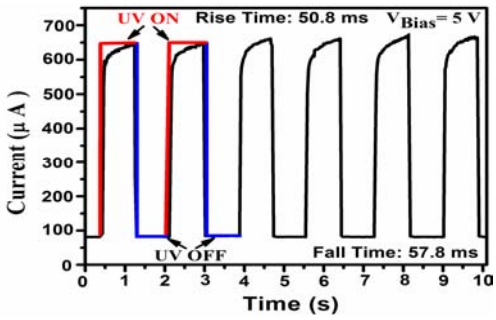

Fig. 10. The repeatability property (ON/OFF) of the TiO_2NRs/p-Si (111) heterojunction photodiode under pulsed UV light (325 nm, 1.6 m W/cm^2).

4. Conclusions

The effects of durations of growth (1, 2, 3, and 4 h) on rutile TiO_2 Ns grown on p-type (111)-oriented silicon substrates were investigated. The duration of growth was found to affect the structural, morphological, and optical properties of TiO_2Ns. uniform and high-density growth mix of NRs and nanoflowers emerged, with each petal of the nanoflowers assembled by several conical rods. All prepared samples fully fit well with the rutile TiO_2 phase (JCPDS card No.01-078-1508). XRD diffraction analysis indicated that TiO_2 at 3 h had the optimal structural properties with the highest (110) peak intensity. In addition, Raman spectra depicted the rutile crystal phase of TiO_2, and the sharpest (smallest FWHMs) and highest peak revealed the high quality of TiO_2Ns with few defects. The PD_i fabricated based on rutile TiO_2/Si was evaluated in the UV region, which demonstrated excellent stability over time, high photocurrent, good sensitivity, and high responsivity. Furthermore, the device showed fast response and recovery time. All of these results demonstrated that high-quality PD_i can be a promising candidate as a low-cost UV photodetector for commercially integrated photoelectronic applications.

Acknowledgements

This work was supported by FRGS grant (203/PFIZIK/6711353), PRGS grant (1001/PFIZIK/846073) and UniversitiSains Malaysia.

References

[1] D. Mardare, M. Tasca, M. Delibas, G. Rusu, On the structural properties and optical transmittance of TiO_2 rf sputtered thin films, Applied Surface Science, 156 (2000) 200-206.

[2] L. C. Chuang, C. H. Luo, S.h. Yang, The structure and mechanical properties of thick rutile–TiO_2 films using different coating treatments, Applied Surface Science, 258 (2011) 297-303.

[3] J. Szczyrbowski, G. Bräuer, M. Ruske, J. Bartella, J. Schroeder, A. Zmelty, Some properties of TiO_2 layers prepared by medium frequency reactive sputtering, Surface and coatings technology, 112 (1999) 261-266.

[4] Z. Han, J. Wang, L. Liao, H. Pan, S. Shen, J. Chen, Phosphorus doped TiO_2 as oxygen sensor with low operating temperature and sensing mechanism, Applied Surface Science, 273 (2013) 349-356.

[5] V. Caratto, B. Aliakbarian, A.A. Casazza, L. Setti, C. Bernini, P. Perego, M. Ferretti, Inactivation of Escherichia coli on anatase and rutile nanoparticles using UV and fluorescent light, Materials Research Bulletin, 48 (2013) 2095-2101.

[6] C. J. Li, G. R. Xu, B. Zhang, J.R. Gong, High selectivity in visible-light-driven partial photocatalytic oxidation of benzyl alcohol into benzaldehyde over single-crystalline rutile TiO_2 nanorods, Applied Catalysis B: Environmental, 115 (2012) 201-208.

[7] C. S. Chou, R.Y. Yang, M.H. Weng, C.H. Yeh, Preparation of TiO_2/dye composite particles and their applications in dye-sensitized solar cell, Powder Technology, 187 (2008) 181-189.

[8] L. Hou, P. Liu, Y. Li, C. Wu, Enhanced performance in organic light-emitting diodes by sputtering TiO_2 ultra-thin film as the hole buffer layer, Thin Solid Films, 517 (2009) 4926-4929.

[9] C. Cao, C. Hu, X. Wang, S. Wang, Y. Tian, H. Zhang, UV sensor based on TiO_2 nanorod arrays on FTO thin film, Sensors and Actuators B: Chemical, 156 (2011) 114-119.

[10] A. MortezaAli, S. R. Sani, Study of growth parameters on structural properties of TiO_2 nanowires, Journal of Nanostructure in Chemistry, 3 (2013) 35.

[11] Q. Zhu, J. Chen, M. Xu, S. Tian, H. Pan, J. Qian, X. Zhou, Microsphere assembly of rutile TiO_2 hierarchically hyperbranched nanorods: CdS sensitization and photovoltaic properties, Solid State Sciences, 13 (2011) 1299-1303.

[12] Z. Luo, W. Yang, A. Peng, Y. Zeng, J. Yao, The fabrication of TiO_2 nanorods from TiO_2 nanoparticles by organic protection assisted template method, Nanotechnology, 20 (2009) 345601.

[13] Z. Liu, C. Liu, J. Ya, E. Lei, Controlled synthesis of ZnO and TiO_2 nanotubes by chemical method and their application in dye-sensitized solar cells, Renewable Energy, 36 (2011) 1177-1181.

[14] S. K. Pradhan, P.J. Reucroft, F. Yang, A. Dozier, Growth of TiO_2 nanorods by metalorganic chemical vapor deposition, Journal of Crystal Growth, 256 (2003) 83-88.

[15] M. S. Wu, C. H. Tsai, T. C. Wei, Electrochemical formation of transparent nanostructured TiO_2 film as an effective bifunctional layer for dye-sensitized solar cells, Chemical Communications, 47 (2011) 2871-2873.

[16] A. More, T. Gujar, J. Gunjakar, C. Lokhande, O. S. Joo, Growth of TiO_2 nanorods by chemical bath deposition method, Applied surface science, 255 (2008) 2682-2687.

[17] U. M. Patil, S. B. Kulkarni, P. R. Deshmukh, R. R. Salunkhe, C.D. Lokhande, Photosensitive nanostructured TiO_2 grown at room temperature by novel "bottom-up" approached CBD method, Journal of Alloys and Compounds, 509 (2011) 6196-6199.

[18] T. Suwannaruang, K. Rivera, A. Neramittagapong, K. Wantala, Effects of hydrothermal temperature and time on uncalcined TiO_2 synthesis for reactive red 120 photocatalytic degradation, Surface and Coatings Technology, (2014).

[19] Y. Zhao, X. Gu, Y. Qiang, Influence of growth time and annealing on rutile TiO_2single-crystal nanorod arrays synthesized by hydrothermal method in dye-sensitized solar cells, Thin Solid Films, 520 (2012) 2814-2818.

[20] D. Regonini, F. Clemens, Anodized TiO_2 Nanotubes: Effect of anodizing time on film length, morphology and photoelectrochemical properties, Materials Letters, 142 (2015) 97-101.

[21] M. Altomare, M. Pozzi, M. Allieta, L.G. Bettini, E. Selli, H_2 and O_2 photocatalytic production on TiO_2 nanotube arrays: effect of the anodization time on structural features and photoactivity, Applied Catalysis B: Environmental, 136 (2013) 81-88.

[22] A. Bandgar, S. Sabale, S. Pawar, Studies on influence of reflux time on synthesis of nanocrystalline TiO_2 prepared by peroxotitanate complex solutions, Ceramics International, 38 (2012) 1905-1913.

[23] H. Cheng, J. Ma, Z. Zhao, L. Qi, Hydrothermal preparation of uniform nanosize rutile and anatase particles, Chemistry of Materials, 7 (1995) 663-671.

[24] J. Zou, Q. Zhang, K. Huang, N. Marzari, Ultraviolet photodetectors based on anodic TiO_2 nanotube arrays, The Journal of Physical Chemistry C, 114 (2010) 10725-10729.

[25] S. Aksoy, Y. Caglar, Structural transformations of TiO_2 films with deposition temperature and electrical properties of nanostructure n-TiO_2/p-Si heterojunction diode, Journal of Alloys and Compounds, 613 (2014) 330-337.

[26] Y.-H. Chang, C.-M. Liu, C. Chen, H.-E. Cheng, The heterojunction effects of TiO_2 nanotubes fabricated by atomic layer deposition on photocarrier transportation direction, Nanoscale research letters, 7 (2012) 1-7.

[27] D. Zhang, X. Gu, F. Jing, F. Gao, J. Zhou, S. Ruan, High performance ultraviolet detector based on TiO_2/ZnO heterojunction, Journal of Alloys and Compounds, 618 (2015) 551-554.

[28] A.M. Selman, Z. Hassan, M. Husham, Structural and photoluminescence studies of rutile TiO_2 nanorods prepared by chemical bath deposition method on Si substrates at different pH values, Measurement, 56 (2014) 155-162.

[29] A. M. Selman, Z. Hassan, Effects of variations in precursor concentration on the growth of rutile TiO_2 nanorods on Si substrate with fabricated fast-response metal–semiconductor–metal UV detector, Optical Materials, 44 (2015) 37-47.

[30] A. M. Selman, Z. Hassan, Growth and characterization of rutile TiO_2 nanorods on various substrates with fabricated fast-response metal–semiconductor–metal UV detector based on Si substrate, Superlattices and Microstructures, 83 (2015) 549-564.

[31] A. M. Selman, Z. Hassan, M. Husham, N. M. Ahmed, A high-sensitivity, fast-response, rapid-recovery p–n heterojunction photodiode based on rutile TiO_2 nanorod array on p-Si (111), Applied Surface Science, 305 (2014) 445-452.

[32] A. M. Selman, Z. Hassan, Highly sensitive fast-response UV photodiode fabricated from rutile TiO_2 nanorod array on silicon substrate, Sensors and Actuators A: Physical, 221 (2015) 15-21.

[33] A. M. Selman, Z. Hassan, Influence of deposition temperature on the growth of rutile TiO_2 nanostructures by CBD method on seed layer prepared by RF magnetron sputtering, Superlattices and Microstructures, 64 (2013) 27-36.

[34] S. K. Gupta, J. Singh, K. Anbalagan, P. Kothari, R.R. Bhatia, P. K. Mishra, V. Manjuladevi, R. K. Gupta, J. Akhtar, Synthesis, phase to phase deposition and characterization of rutile nanocrystalline titanium dioxide (TiO_2) thin films, Applied Surface Science, 264 (2013) 737-742.

[35] N. R. Mathews, E. R. Morales, M. A. Cortés-Jacome, J. A. Toledo Antonio, TiO_2 thin films – Influence of annealing temperature on structural, optical and photocatalytic properties, Solar Energy, 83 (2009) 1499-1508.

[36] J. J. Yuan, H. D. Li, S.Y. Gao, D. D. Sang, L.A. Li, D. Lu, Hydrothermal synthesis, characterization and properties of TiO_2 nanorods on boron-doped diamond film, Materials Letters, 64 (2010) 2012-2015.

[37] B. Choudhury, A. Choudhury, Local structure modification and phase transformation of TiO_2 nanoparticles initiated by oxygen defects, grain size, and annealing temperature, International Nano Letters, 3 (2013) 55.

[38] J. Archana, M. Navaneethan, Y. Hayakawa, Hydrothermal growth of monodispersed rutile TiO_2 nanorods and functional properties, Materials Letters, 98 (2013) 38-41.

[39] Y. Han, G. Li, Z. Zhang, Synthesis and optical properties of rutile TiO_2 microspheres composed of radially aligned nanorods, Journal of Crystal Growth, 295 (2006) 50-53.

[40] Q. Gao, X. Wu, Y. Fan, X. Zhou, Low temperature fabrication of nanoflower arrays of rutile TiO_2 on mica particles with enhanced photocatalytic activity, Journal of Alloys and Compounds, 579 (2013) 322-329.

[41] J. Zhou, G. Zhao, G. Han, B. Song, Solvothermal growth of three-dimensional TiO_2 nanostructures and their optical and photocatalytic properties, Ceramics International, 39 (2013) 8347-8354.

[42] D. Dubal, D. Dhawale, A. More, C. Lokhande, Synthesis and characterization of photosensitive TiO_2 nanorods by controlled precipitation route, Journal of materials science, 46 (2011) 2288-2293.

[43] H. Nakajima, T. Mori, Q. Shen, T. Toyoda, Photoluminescence study of mixtures of anatase and rutile TiO_2 nanoparticles: Influence of charge transfer between the nanoparticles on their photoluminescence excitation bands, Chemical Physics Letters, 409 (2005) 81-84.

[44] W. Zhang, J. Zhao, Z. Liu, Z. Liu, Z. Fu, Influence of growth temperature of TiO_2 buffer on structure and PL properties of ZnO films, Applied Surface Science, 256 (2010) 4423-4425.

[45] J. Preclíková, P. Galář, F. Trojánek, B. Rezek, Y. Němcová, P. Malý, Photoluminescence of nanocrystalline titanium dioxide films loaded with silver nanoparticles, Journal of Applied Physics, 109 (2011) 083528.

[46] M. Vishwas, K. Narasimha Rao, R. Chakradhar, Influence of annealing temperature on Raman and photoluminescence spectra of electron beam evaporated TiO_2 thin films, Spectrochimica Acta Part A: Molecular and Biomolecular Spectroscopy, 99 (2012) 33-36.

[47] H. Tang, H. Berger, P.E. Schmid, F. Lévy, Optical properties of anatase (TiO_2), Solid State Communications, 92 (1994) 267-271.

[48] J. Shi, J. Chen, Z. Feng, T. Chen, Y. Lian, X. Wang, C. Li, Photoluminescence characteristics of TiO_2 and their relationship to the photoassisted reaction of water/methanol mixture, The journal of physical chemistry C, 111 (2007) 693-699.

[49] X. Shen, J. Zhang, B. Tian, Microemulsion-mediated solvothermal synthesis and photocatalytic properties of crystalline titania with controllable phases of anatase and rutile, Journal of hazardous materials, 192 (2011) 651-657.

[50] L. Dong, K. Cheng, W. Weng, C. Song, P. Du, G. Shen, G. Han, Hydrothermal growth of rutile TiO_2 nanorod films on titanium substrates, Thin Solid Films, 519 (2011) 4634-4640.

[51] R. Chen, M. Wang, Synthesis of hierarchical TiO_2 micro/nanostructure and its application in hybrid solar cell, Materials Letters, 69 (2012) 41-44.

[52] Y. Fu, W. Cao, Preparation of transparent TiO_2 nanocrystalline film for UV sensor, Chinese Science Bulletin, 51 (2006) 1657-1661.

[53] B. E. A. Saleh, M. C. Teich, Semiconductor Photon Detectors, in: Fundamentals of Photonics, John Wiley & Sons, Inc., 2001, pp. 644-695.

[54] N. K. Hassan, M. R. Hashim, N. K. Allam, Low power UV photodetection characteristics of cross-linked ZnO nanorods/nanotetrapods grown on silicon chip, Sensors and Actuators A: Physical, 192 (2013) 124-129.

[55] J. J. Hassan, M. A. Mahdi, C. W. Chin, Z. Hassan, H. Abu-Hassan, Microwave assisted chemical bath deposition of vertically aligned ZnO nanorods on a variety of substrates seeded by PVA–Zn(OH)2 nanocomposites, Applied Surface Science, 258 (2012) 4467-4472.

[56] N. Al-Hardan, M. Abdullah, N. Ahmed, F. Yam, A. A. Aziz, UV photodetector behavior of 2D ZnO plates prepared by electrochemical deposition, Superlattices and Microstructures, 51 (2012) 765-771.

[57] X. Kong, C. Liu, W. Dong, X. Zhang, C. Tao, L. Shen, J. Zhou, Y. Fei, S. Ruan, Metal-semiconductor-metal TiO2 ultraviolet detectors with Ni electrodes, Applied Physics Letters, 94 (2009) 123502.

[58] L. Hu, J. Yan, M. Liao, H. Xiang, X. Gong, L. Zhang, X. Fang, An Optimized Ultraviolet‐A Light Photodetector with Wide‐Range Photoresponse Based on ZnS/ZnO Biaxial Nanobelt, Advanced Materials, 24 (2012) 2305-2309.

[59] N. Naderi, M. Hashim, Porous-shaped silicon carbide ultraviolet photodetectors on porous silicon substrates, Journal of Alloys and Compounds, 552 (2013) 356-362.

[60] F. H. Babaei, M. M. Lajvardi, F.A. Boroumand, Large area Ag–TiO_2 UV radiation sensor fabricated on a thermally oxidized titanium chip, Sensors and Actuators A: Physical, 173 (2012) 116-121.

[61] N. Hassan, M. Hashim, Flake-like ZnO nanostructures density for improved absorption using electrochemical deposition in UV detection, Journal of Alloys and Compounds, 577 (2013) 491-497.

[62] H. Xue, X. Kong, Z. Liu, C. Liu, J. Zhou, W. Chen, S. Ruan, Q. Xu, TiO_2 based metal-semiconductor-metal ultraviolet photodetectors, Applied physics letters, 90 (2007) 201118-201118-201113.

[63] D. Çalışkan, B. Bütün, Ş. Özcan, E. Özbay, Metal–semiconductor–metal photodetector on as-deposited TiO_2 thin films on sapphire substrate, Journal of Vacuum Science & Technology B, 31 (2013) 020606.

[64] W. J. Lee, M. H. Hon, An ultraviolet photo-detector based on TiO_2/water solid-liquid heterojunction, Applied Physics Letters, 99 (2011) 251102.

[65] C. M. Liu, C. Chen, H. E. Cheng, Ultraviolet Photoresponse of TiO_2 Nanotube Arrays Fabricated by Atomic Layer Deposition, Electrochemical and Solid-State Letters, 14 (2011) K33-K35.